Journal of Physics: Condensed Matter

PAPER

Ferroelectric and dipole control of band alignment in the two dimensional $InTe/In_2Se_3$ heterostructure

To cite this article: Bin Zhou *et al* 2020 *J. Phys.: Condens. Matter* **32** 055703

View the article online for updates and enhancements.

IOP ebooks™

Bringing you innovative digital publishing with leading voices to create your essential collection of books in STEM research.

Start exploring the collection - download the first chapter of every title for free.

This content was downloaded from IP address 222.204.248.6 on 02/11/2019 at 12:56

IOP Publishing

Journal of Physics: Condensed Matter

J. Phys.: Condens. Matter **32** (2020) 055703 (8pp)

https://doi.org/10.1088/1361-648X/ab4d60

Ferroelectric and dipole control of band alignment in the two dimensional InTe/In_2Se_3 heterostructure

Bin Zhou[1], Shi-Jing Gong[2], Kai Jiang[1], Liping Xu[1], Liangqing Zhu[1], Liyan Shang[1], Yawei Li[1], Zhigao Hu[1,3,4] and Junhao Chu[1,3,4]

[1] Technical Center for Multifunctional Magneto-Optical Spectroscopy (Shanghai), Department of Materials, School of Physics and Electronic Science, East China Normal University, Shanghai 200241, People's Republic of China

[2] Key Laboratory of Polar Materials and Devices (MOE), East China Normal University, Shanghai 200241, People's Republic of China

[3] Collaborative Innovation Center of Extreme Optics, Shanxi University, Taiyuan, Shanxi 030006, People's Republic of China

[4] Shanghai Institute of Intelligent Electronics & Systems, Fudan University, Shanghai 200433, People's Republic of China

E-mail: sjgong@ee.ecnu.edu.cn and zghu@ee.ecnu.edu.cn

Received 19 June 2019, revised 28 September 2019
Accepted for publication 14 October 2019
Published 1 November 2019

Abstract

Two dimensional (2D) ferroelectric materials are gaining growing attention due to their nontrival ferroelectricity, and the 2D ferroelectric heterostructures with tunable electronic, optoelectronic, or even magnetic properties, show many novel properties that do not exist in their constituents. In this work, by using the first-principles calculations, we investigate the ferroelectric and dipole control of electronic structures of the 2D ferroelectric heterostructure InTe/In_2Se_3. It is found that band alignment is closely dependent on the ferroelectric polarization of In_2Se_3. By switching the polarization of In_2Se_3, the band alignment of InTe/In_2Se_3 switches from a staggered (type II) to a straddling type (type I) , and the band gap changes from indirect gap 0.76 eV to direct gap 0.15 eV. When the ferroelectric field of In_2Se_3 is reversed, the band alignment of InTe/In_2Se_3 switches from type-I to type-II, and the band gap changes from indirect gap 0.76 eV to direct gap 0.15 eV. In addition, we find that the interlayer dipole can also effectively modulate the band structure and induce the type-I to type-II band alignment transition. Our present results indicate that the 2D ferroelectric heterostructure with the tunable band alignment and band gap can be of great significance in the optoelectronic devices.

Keywords: InTe/In_2Se_3 heterostructure, two dimensional ferroelectric, the first-principles calculations, electronic structures

(Some figures may appear in colour only in the online journal)

1. Introduction

Two dimensional (2D) materials have attracted wide research interest, due to their novel physical properties and promising applications in optoelectronics, valleytronics, and spintronics, *et al* [1–4]. Many 2D materials have been isolated from their bulk counterparts, such as silicene [5, 6], phosphorene [7–9], transition metal chalcogenides (TMDCs) [10–12], and III–VI binary compounds (e.g. In_2Se_3) [13–15]. The 2D heterostructures, which combine two or more layered materials with weak van der Waals (vdW) interactions, provide new properties that do not exist in their individual constituent [16–18]. So far, a variety of 2D heterostructures, such as MoS_2/phosphorene [19, 20], graphene/BN [21], WS_2/C_2N [22], etc have

© 2019 IOP Publishing Ltd Printed in the UK

been studied. For example, Deng *et al* [19] reported that the photodetection responsivity of black phosphorus/MoS_2 heterostructure improves nearly 100 times than the single black phosphorus phototransistor.

The electric control of band alignment in heterostructure has been studied extensively [23, 24]. Tunable band alignment offers potential technological applications in optoelectronic devices. For example, the type-I semiconductor, in which both the valence and the conduction band edges of the one components are localized within the energy gap of the other material of the heterostructure, can achieve high emission quantum yields (QY), as well as enhanced photostability [25]. While for type-II heterostructures, in which their relative band-edge positions form a staggered band alignment, whereby the hole is located in the one component and the electron is located in the other component, thus a charge carrier separation occurs. However, directly applying the electric field in laboratory is usually low efficiency and high energy consumption. Alternatively, in 2D ferroelectric heterostrucrue, the ferroelectric polarization may be used for tuning the electronic structure [26–28]. The stable of room-temperature ferroelectricity of thin film In_2Se_3 has been confirmed both in theory and experiments [29–32]. The electronic properties of single- and few-layer In_2Se_3 has been investigated theoretically using the first-principles calculations [32, 33]. Ding *et al* [32] demonstrated that the 2D ferroelectric heterostructure In_2Se_3/graphene can exhibit a tunable Schottky barrier, and In_2Se_3/WSe_2 heterostructure displays a rapid band gap reduction in the combined 2D ferroelectric system. Compared to the external electric field, the intrinsic electric field induced by the ferroelectric polarization at the interface may reach 1 GV m^{-1} [26], which is much larger than the electric field produced in experiment conditions [34, 35]. The bistable polarization of the ferroelectric is nonvolatile and can be easily reversed at a relatively low voltages, which provides large and switchable electric fields.

In this paper, we construct $InTe/In_2Se_3$ heterostructures and investigate their electronic structures and band alignment. The results reveal that the band alignment of $InTe/In_2Se_3$ can be switched between type-I and type-II when the ferroelectric field is reversed. Meanwhile, the band gap changes from indirect gap to direct gap and show a rapid band reduction. Also, the transition from type-I to type-II band alignment can be induced through interlayer dipole. These results indicate that the ferroelectric heterostructures with tunable band alignment and band gap can be significance in application of nanoscaled optoelectronic devices.

2. Computational details

All calculations are executed based on density-functional theory (DFT) in conjunction with the projector-augmented-wave (PAW) method as implemented by the Vienna *ab initio* simulation package (VASP) code [36, 37]. The electron exchange and correlation are described by the Perdew–Burke–Ernzerhof (PBE) function with generalized gradient approximation (GGA) [38–40]. The energy cutoff is 500 eV, and k-point sampling is done by choosing the Monkhorst–Pack mesh scheme with $15 \times 15 \times 1$ [41]. The weak vdW interaction between layers is described by semi-empirical DFT-D3 method. A vacuum slab larger than 20 Å is used along z direction to avoid the interaction between the neighboring layers. Because of the asymmetric layer arrangement, the dipole correction is employed. All initial geometry structures are fully relaxed until the convergence criteria of energy and force are less than 10^{-6} eV and 0.01 eV Å^{-1}, respectively. To quantitative evaluation the stability of the heterostructures, we calculate the binding energy E_b using the following: $E_b = E_{InTe/In_2Se_3} - (E_{In_2Se_3} + E_{InTe})$ where E_{InTe/In_2Se_3}, $E_{In_2Se_3}$, and E_{InTe} represent the total energies of the $InTe/In_2Se_3$ heterostructure, In_2Se_3 and InTe monolayers, respectively.

3. Results and discussion

We construct $InTe/In_2Se_3$ heterostructures considering two different ferroelectric field direction, as shown in figure 1(a), labeled as $InTe/In_2Se_3$(I) and $InTe/In_2Se_3$(II). The $InTe/In_2Se_3$(I) are heterostructure with the out-of-plane ferroelectric field F_E points from InTe layer to In_2Se_3 layer. For $InTe/In_2Se_3$(II), the ferroelectric field F_E is reversed. The interface electric fields for two stackings are denoted by $E_{int\text{-}I}$ and $E_{int\text{-}II}$, respectively. For I stacking, the ferroelectric field F_E is opposite to the interface electric field $E_{int\text{-}I}$. For II stacking, the ferroelectric field F_E is the same as the interface electric field $E_{int\text{-}II}$. We first optimize the lattice parameters of the monolayer In_2Se_3 and InTe based on the minimization of the total energy. The calculated lattice parameters is $a = b = 4.09$ Å for In_2Se_3, $a = b = 4.39$ Å for InTe monolayer. These results are well consistent with previous theoretical and experimental values [32, 33, 42]. Because of their close lattice constants, $InTe/In_2Se_3$ heterostructures are built with unit cells containing nine atoms in total. The lattice mismatch are less than 4%, which is in a reasonable range. The optimized lattice parameters, band gap as well as the work function of $InTe/In_2Se_3$ for two different stacking configurations are summarized in table 1. It is interesting that the $InTe/In_2Se_3$(II) configuration has more negative binding energy compared to the other configuration, as shown in figure 1(b), which indicates that the II stacking is more stable than I stacking. The both negative binding energies indicate that the considered two stacking configurations are energetically stable.

The intrinsic dipole is 0.10 eÅ for In_2Se_3 monolayer, which agrees well with the previous results [32]. The intrinsic dipole introduces an electrostatic potential difference $\Delta\Phi = 1.34$ eV between the two surface within In_2Se_3 monolayer as shown in figure 2(a). As showed in figures 2(b) and (c), the electrostatic potential differences between InTe layer and In_2Se_3 layer is 1.06 eV for $InTe/In_2Se_3$(I), 0.62 eV for $InTe/In_2Se_3$(II), respectively. The decrease of the dipole moment and electrostatic potential differences in $InTe/In_2Se_3$(II) can be attributed to the screening effects [43–45] due to the charge transfer and depolarizing electrostatic field between the two layers in heterostructure.

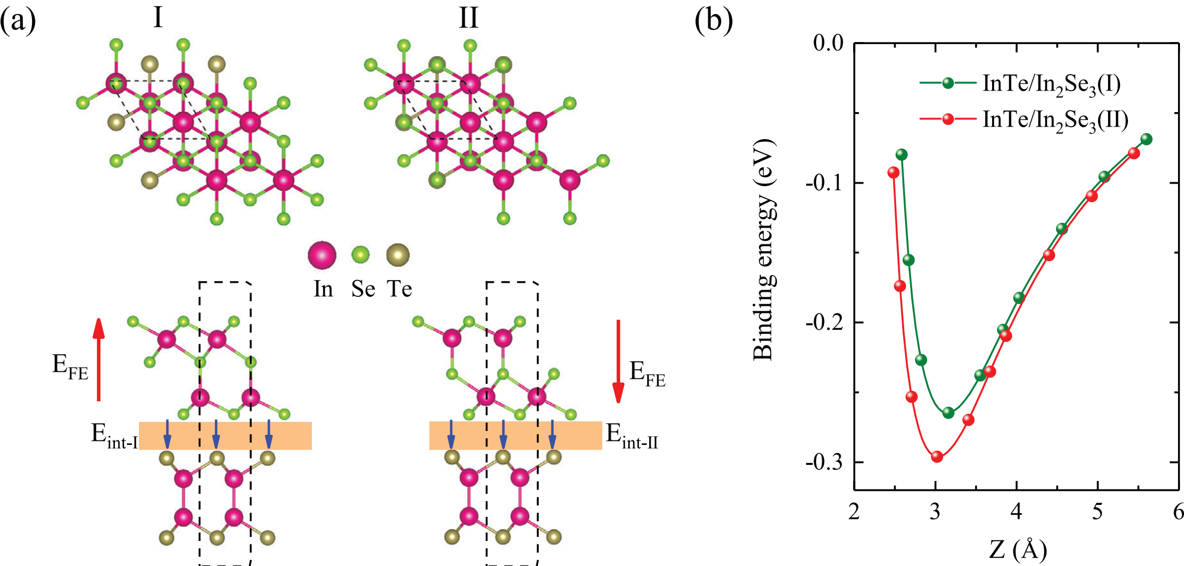

Figure 1. (a) The top and side view of the InTe/In_2Se_3 heterostructures with the direction of ferroelectric up and down. (b) The binding energy as a function of interlayer distances for InTe/In_2Se_3(I) and InTe/In_2Se_3(II) heterostructures.

Table 1. The optimized lattice parameters, interlayer distances, interlayer binding energy E_b (per unit cell), workfunction, band gap, dipole moment and the potential differences of the two surfaces $\Delta\Phi$.

	$a = b$ (Å)	Distance (Å)	E_b (meV)	Workfunction (eV)	E_g (eV)	Dipole moment (eÅ)	$\Delta\Phi$ (eV)
In_2Se_3	4.10			5.99, 4.81	0.78	0.10	1.34
InTe	4.39			4.92	1.54	0.00	0.00
InTe/In_2Se_3(I)	4.20	3.16	−266	6.36	0.76	0.16	1.06
InTe/In_2Se_3(II)	4.20	3.02	−296	5.26	0.15	0.09	0.62

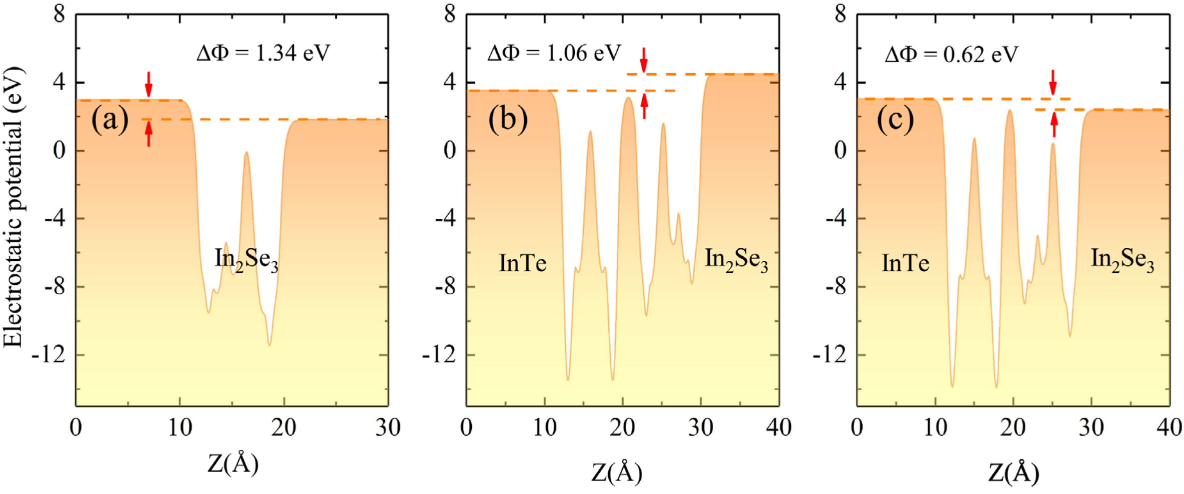

Figure 2. (a) The electrostatic potential for In_2Se_3 monolayer. (b) and (c) The electrostatic potential for InTe/In_2Se_3(I) and InTe/In_2Se_3(II) heterostructures, respectively.

We show the projected band structures of InTe/In_2Se_3(I), InTe/In_2Se_3(II) and the corresponding monolayers in figures 3(a)–(d). For InTe/In_2Se_3(I), it is a type-I semiconductor, while for InTe/In_2Se_3(II), the energy band becomes type-II band alignment. The former has an indirect band gap of about 0.78 eV with the position of conduction band minimum (CBM) located at the Γ point and valence band minimum (VBM) located in the region between the high-symmetry points Γ and M. While the InTe/In_2Se_3(II) has a direct band gap of 0.15 eV with the CBM and VBM both located at the Γ point. In the case of InTe/In_2Se_3(II), the CBM is contributed by In_2Se_3 and VBM is by InTe layer, which indicated that the hole states are localized in the InTe layer, while electron states are contributed by In_2Se_3 layer. For InTe/In_2Se_3(I), it can be seen that the CBM and VBM are both contributed by the In_2Se_3 layer which is suitable for light emission applications. The band alignment

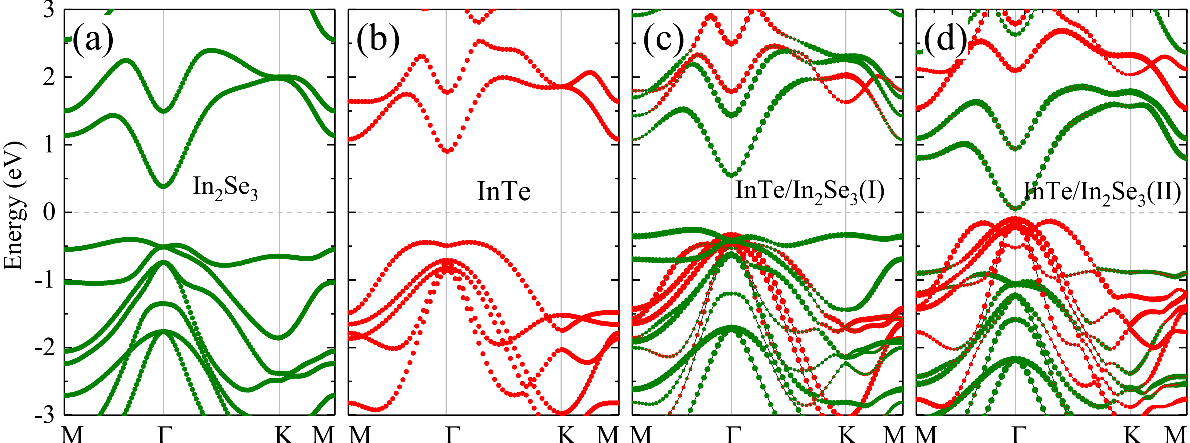

Figure 3. The band structures of (a) InTe and (b) In_2Se_3 monolayers. The projected band structure of (c) $InTe/In_2Se_3$(I) and (d) $InTe/In_2Se_3$(II). The projected band structure dominated by In_2Se_3 and InTe are plotted using dark green and red dots. The size of the dots reflects the proportion of each layer.

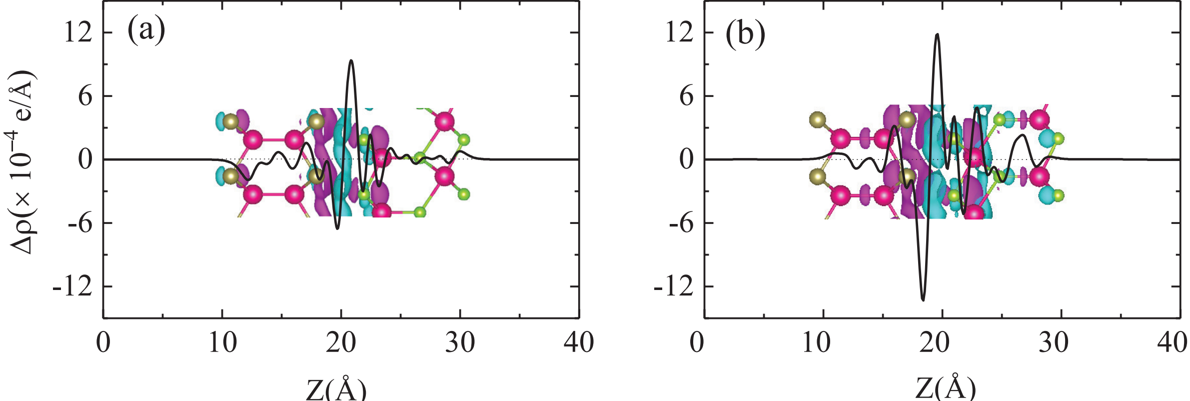

Figure 4. The plane-averaged charge density difference for $InTe/In_2Se_3$(I) and $InTe/In_2Se_3$(II) at equilibrium distance along the z direction. The inset is the 3D surface of the charge density difference with an isosurface value of 0.0001 eÅ^{-3}, the cyan and violet areas represent electron accumulation and depletion, respectively.

transition from type-II to type-I is important to design novel optoelectric devices. These results show that the ferroelectric polarization can effectively modulate the electron and exciton properties of the $InTe/In_2Se_3$ heterostructure.

To visualize the charge redistribution and understand the charge transfer mechanism in $InTe/In_2Se_3$ heterostructures, we show the charge density difference in figures 4(a) and (b). The planar-averaged differential charge density is calculated by using $\Delta\rho(z) = \int \rho_{\mathrm{Hetero}}(x,y,z)\mathrm{d}x\mathrm{d}y - \int \rho_{\mathrm{InTe}}(x,y,z)\mathrm{d}x\mathrm{d}y - \int \rho_{\mathrm{In_2Se_3}}(x,y,z)\mathrm{d}x\mathrm{d}y$, where $\rho_{\mathrm{Hetero}}(x,y,z)$, $\rho_{\mathrm{InTe}}(x,y,z)$ and $\rho_{\mathrm{In_2Se_3}}(x,y,z)$ are the charge density at the (x,y,z) point in $InTe/In_2Se_3$ heterobilayer, InTe and In_2Se_3 monolayers, respectively. We can see that the charge redistribution is mainly between Te atoms and adjacent Se atoms at interface. For both $InTe/In_2Se_3$ heterostructures, it can be seen that the charge is depleted on the InTe side (violet area) and accumulated in the In_2Se_3 layer (cyan area), thus a remarkable charge rearrangement occurs at the interface of the hybrid structure. We further perform charge analysis based on the Bader method [46] and gained the exact transferred electrons of interlayer, which is 0.014 e and 0.027 e for $InTe/In_2Se_3$(I) and $InTe/In_2Se_3$(II), respectively. The more transferred electrons in $InTe/In_2Se_3$(II) indicates a much stronger interlayer interaction than $InTe/In_2Se_3$(I), therefore, results a more negative binding energy.

The band alignment of semiconductor is significance in designing novel optoelectronic devices [47]. Here, the band alignment of the In_2Se_3 monolayer, InTe monolayer, and $InTe/In_2Se_3$ heterostructures are showed in figure 5. Furthermore, to evaluate the carriers confnement effect, we define the conduction (valence) band offset (CBO, VBO) as $\triangle E_{\mathrm{C}} = |E_{\mathrm{C(In_2Se_3)}} - E_{\mathrm{C(InTe)}}|$ ($\triangle E_{\mathrm{V}} = |E_{\mathrm{V(In_2Se_3)}} - E_{\mathrm{V(InTe)}}|$). For $InTe/In_2Se_3$(I) heterostructure, the CBO and VBO of the $InTe/In_2Se_3$(II) are 0.88 eV and 0.05 eV. Such a tiny VBO make it is easy to relaize the switching between Type-I and Type-II band alignment which can be used to design novel optoelectronic devices. The conduction band offset and the valence band offset of the $InTe/In_2Se_3$(II) are 1.36 eV and 0.85 eV, respectively. Such a large band offset will prolong the lifetime of interlayer exciton [48], which is crucial for improve the efficiency of carrier separation.

Next, we turn to discuss the influence of the interlayer coupling effect. The coupling effects of InTe and In_2Se_3 monolayers in the heterostructure can be modulated effectively through adjusting interlayer distance, thus the interlayer

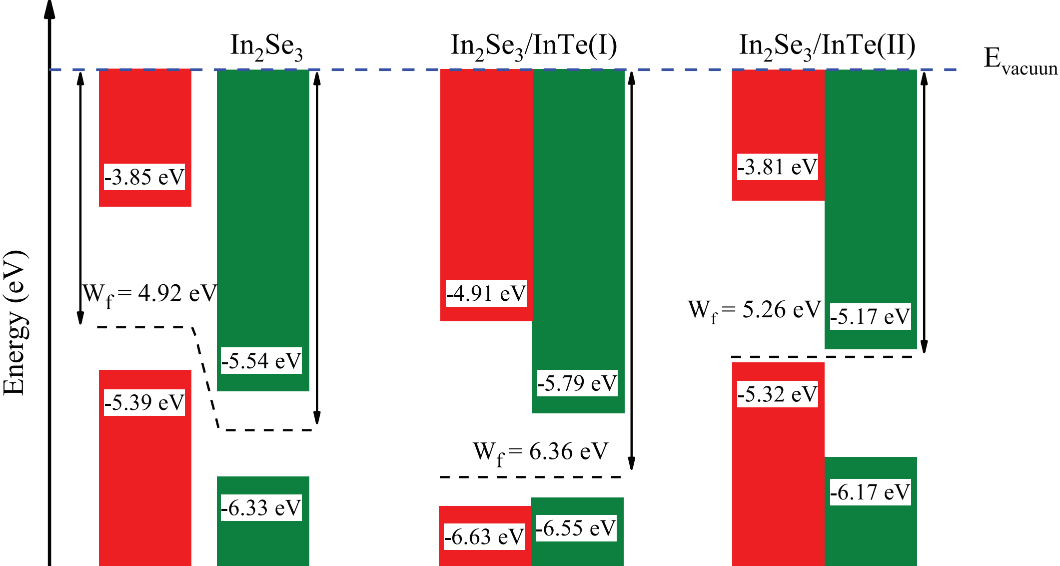

Figure 5. Band alignments of monolayer InTe, monolayer In_2Se_3 and InTe/In_2Se_3 heterostructures. The horizontal dark dashed lines are the Fermi level. The vacuum level is taken as reference.

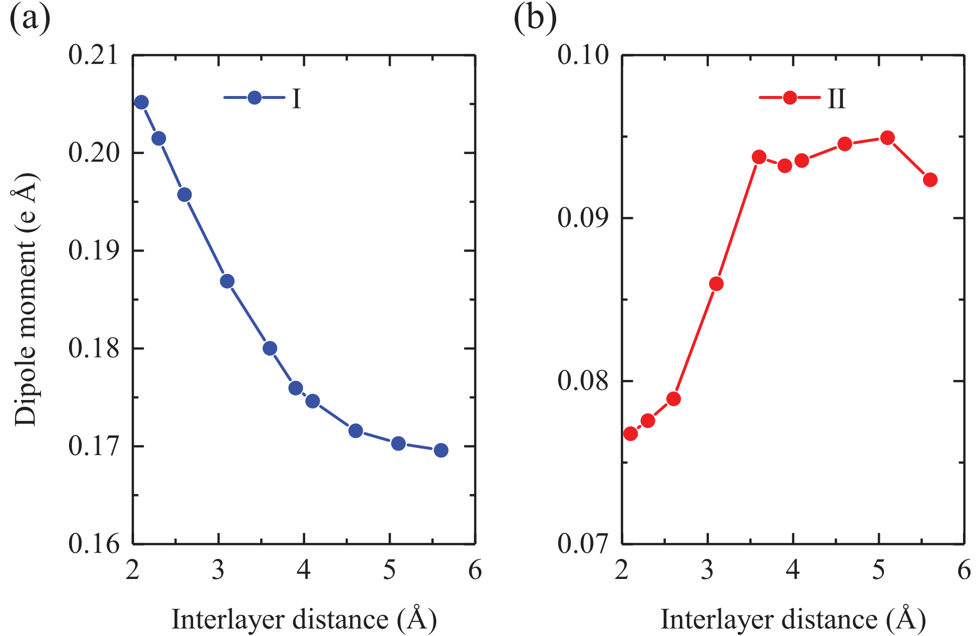

Figure 6. The magnitude of dipole moment at different interlayer distances for (a) InTe/In_2Se_3(I) and (b) InTe/In_2Se_3(II).

dipole is controled. To investigate the tunable effects of interlayer coupling, we vary the distances between InTe and In_2Se_3 for InTe/In_2Se_3(I) from 2 Å to 5.5 Å, then fully relax the structure to acquire the accurate electronic properties. As we see in figures 6(a) and (b), the magnitude of the electric dipole for two heterostructure both change obviously with the variation of interlayer distance, which indicates a strongly coupling effect between In_2Se_3 and InTe monolayer. For InTe/In_2Se_3(I) heterostructure, the electric dipole moment is decreased with increased interlayer distance. The electric dipole moment is increased with increasing the interlayer distance for II stacking. The reason is given as follows. For II stacking, the direction of interface electric field $E_{\text{int-II}}$ is the same as the ferroelectric field F_E. The F_E and $E_{\text{int-II}}$ together enhance the electron transfer from InTe layer to In_2Se_3 layer, thus reinforce the electron screening effect in InTe/In_2Se_3(II) heterostructure which counteract the built-in electric field of the ferroelectric layer. When increasing the interlayer distance, the electron screening effect is weaked, therefore increase the magnitude of diople moment. For InTe/In_2Se_3(I), the direction of interface electric field $E_{\text{int-II}}$ is opposite to the ferroelectric field F_E, thus, the electron screening effect is very weak. The monotonously decrease of the dipole moment may be attribute to the increase of thickness of the heterostructure.

In figures 7(a)–(f), we showed the projected band structures of InTe/In_2Se_3(I) for a series of different interlayer distances to deeply understand the evolution mechanism of the electronic structure with variation of interlayer distance. When

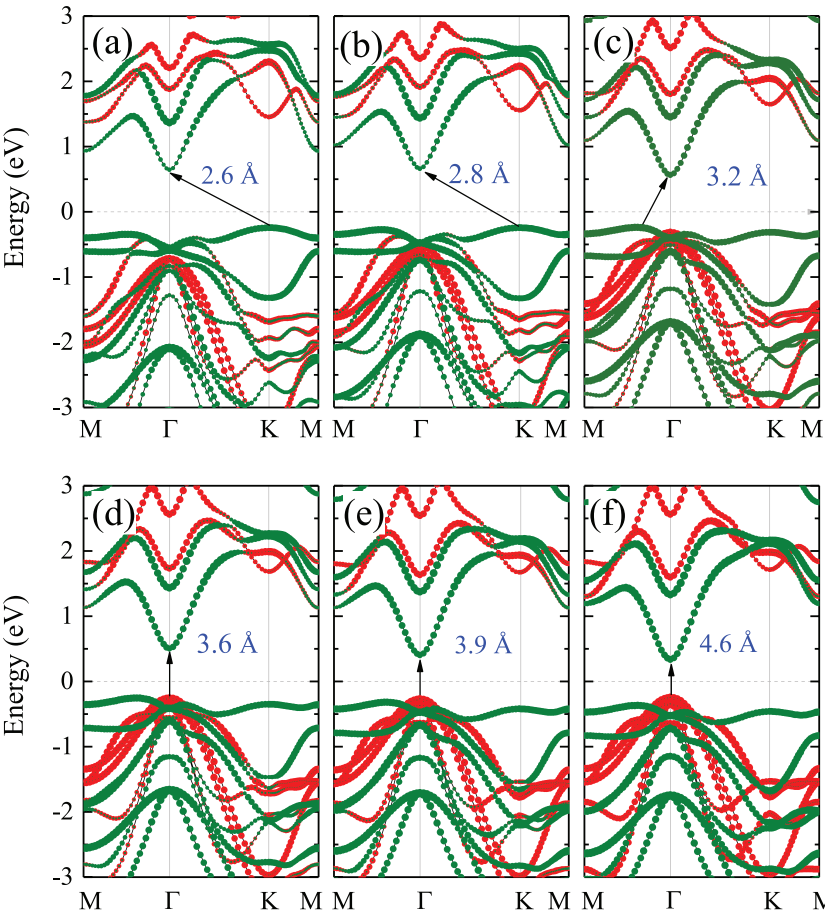

Figure 7. The evolution of projected band structures of InTe/In_2Se_3(I) heterostructure with different interlayer distances 2.6 Å, 2.8 Å, 3.2 Å, 3.6 Å, 3.9 Å, 4.6 Å, and the black arrows indicate the fundamental band gap.

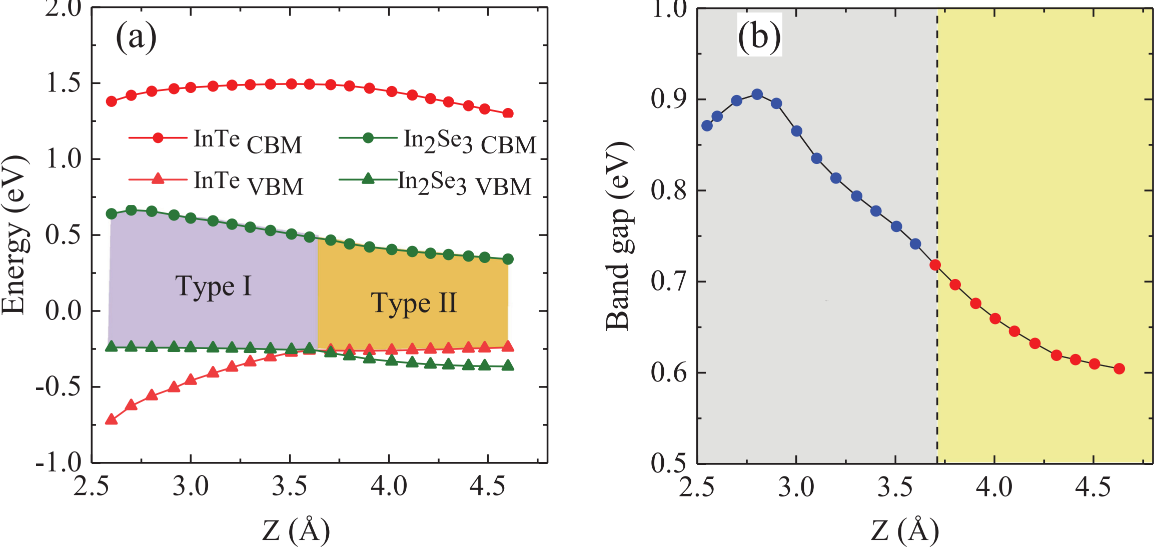

Figure 8. (a) The variation of the band edges with different interlayer distances in InTe/In_2Se_3(I). (b) The corresponding band gap as a function of interlayer distance. In (b), the red circles indicate the direct band gap, and the dark green ones indicate the indirect gap.

the distances are 2.6 Å, 2.8 Å, 3.2 Å, the VBM and CBM are both contributed by In_2Se_3 layer, which demonstrates a typical type-I band alignment. As the distances increase up to 3.6 Å, which is a critical point for the transition from type-I to type-II, the In_2Se_3 contributes to the CBM and the InTe layer contributes to the VBM. The variation of band edge, band gap of InTe/In_2Se_3(I) as a function of interlayer distance are showed in figures 8(a) and (b). It can be seen that the band gap can be modulated effectively by the interlayer distance. The band gap decreases linearly when the distance between two

layers vary from 2.8 Å to 4.6 Å as shown in figure 8(b). While the interlayer distance vary from 2.8 Å to 2.5 Å, the band gap starts to decrease slowly. In figure 8(a), the heterostructure keeps as type-I semiconductor with indirect band gap as the interlayer distance changing from 3.6 Å to 2.5 Å. However, when the interlayer distance increases up to 3.6 Å, the VBM of InTe at the Γ point moves upward and surpass the VBM of In_2Se_3 layer. The InTe/In_2Se_3(II) presents a distinguishing feature of a type-II band alignment. If we continue to increase the interlayer distance, the VBM origins from the InTe almost keep unchange, while the VBM from In_2Se_3 starts to shift down quickly. The results provide a novel and feasible method to control the band alignment by ferroelectric and dipole of the ferroelectric-based heterostructures.

4. Conclusion

In summary, we have theoretically investigated the electronic properties and band alignment of 2D InTe/In_2Se_3 vdW heterostructures through the first-principle calculations. Our results reveal that the out-of-plane ferroelectric field has tunable effect on the band alignment of the heterostructures. For InTe/In_2Se_3(I), it is a type-I band alignment semiconductor with an indirect band gap 0.76 eV. When the ferroelectric polarization is reversed, the band structure becomes type-II with a direct band gap 0.15 eV. Moreover, an intrinsic type-I band alignment can be modulated to type-II band alignment by dipole control. The present results indicate that the ferroelectric heterostructures can pave new ways to control and utilize two-dimensional materials in future optoelectronic devices.

Acknowledgment

This work was financially supported by the National Key R&D Program of China (Grant Nos. 2017YFA0303403 and 2018YFB0406500), the National Natural Science Foundation of China (Grant Nos. 61674057, 61774059, 91833303 and 61974043), the Projects of Science and Technology Commission of Shanghai Municipality (Grant Nos. 18JC1412400, 18YF1407200, and 18YF1407000), and the Program for Professor of Special Appointment (Eastern Scholar) at Shanghai Institutions of Higher Learning.

ORCID iDs

Shi-Jing Gong https://orcid.org/0000-0002-9292-7609
Yawei Li https://orcid.org/0000-0001-8776-5687
Zhigao Hu https://orcid.org/0000-0003-0575-2191

References

[1] Novoselov K S, Geim A K, Morozov S V, Jiang D, Katsnelson M I, Grigorieva I V, Dubonos S V and Firsov A A 2005 Two-dimensional gas of massless Dirac fermions in graphene *Nature* **438** 197–200
[2] Novoselov K S, McCann E, Morozov S V, Falko V I, Katsnelson M I, Zeitler U, Jiang D, Schedin F and Geim A K 2006 Unconventional quantum Hall effect and Berrys phase of 2π in bilayer graphene *Nat. Phys.* **2** 177–80
[3] Han W, Kawakami R K, Gmitra M and Fabian J 2014 Graphene spintronics *Nat. Nanotechnol.* **9** 794
[4] Gong S J, Gong C, Sun Y Y, Tong W Y, Duan C G, Chu J H and Zhang X 2018 Electrically induced 2D half-metallic antiferromagnets and spin field effect transistors *Proc. Natl Acad. Sci. USA* **115** 8511–6
[5] Feng B, Ding Z, Meng S, Yao Y, He X, Cheng P, Chen L and Wu K 2012 Evidence of silicene in honeycomb structures of silicon on Ag (1 1 1) *Nano Lett.* **12** 3507–11
[6] De Padova P, Quaresima C, Ottaviani C, Sheverdyaeva P M, Moras P, Carbone C, Topwal D, Olivieri B, Kara A and Oughaddou H 2010 Evidence of graphene-like electronic signature in silicene nanoribbons *Appl. Phys. Lett.* **96** 261905
[7] Liu H, Neal A T, Zhu Z, Luo Z, Xu X, Tomnek D and Ye P D 2014 Phosphorene: an unexplored 2D semiconductor with a high hole mobility *ACS Nano* **8** 4033–41
[8] Li L, Yu Y, Ye G J, Ge Q, Ou X, Wu H, Feng D, Chen X H and Zhang Y 2014 Black phosphorus field-effect transistors *Nat. Nanotechnol.* **9** 372–7
[9] Watts M C, Picco L, Russell-Pavier F S, Cullen P L, Miller T S, Bartuś S P, Payton O D, Skipper N T, Tileli V and Howard C A 2019 Production of phosphorene nanoribbons *Nature* **568** 216
[10] Barrera D, Wang Q, Lee Y-J, Cheng L, Kim M J, Kim J and Hsu J W P 2017 Solution synthesis of few-layer 2H MX_2 (M = Mo, W; X = S, Se) *J. Mater. Chem.* C **5** 2859–64
[11] Wang F, Wang J, Guo S, Zhang J, Hu Z and Chu J 2017 Tuning coupling behavior of stacked heterostructures based on MoS_2, WS_2, and WSe_2 *Sci. Rep.* **7** 44712
[12] Yao Q-F, Cai J, Tong W-Y, Gong S-J, Wang J-Q, Wan X, Duan C-G and Chu J 2017 Manipulation of the large Rashba spin splitting in polar two-dimensional transition-metal dichalcogenides *Phys. Rev.* B **95** 165401
[13] Zhou J, Zeng Q, Lv D, Sun L, Niu L, Fu W, Liu F, Shen Z, Jin C and Liu Z 2015 Controlled synthesis of high-quality monolayered α-In_2Se_3 via physical vapor deposition *Nano Lett.* **15** 6400–5
[14] Tao X and Gu Y 2013 Crystalline-Crystalline phase transformation in two-dimensional In_2Se_3 thin layers *Nano Lett.* **13** 3501–5
[15] Lin M, Wu D, Zhou Y, Huang W, Jiang W, Zheng W, Zhao S, Jin C, Guo Y and Peng H 2013 Controlled growth of atomically thin In_2Se_3 flakes by van der Waals epitaxy *J. Am. Chem. Soc.* **135** 13274–7
[16] Britnell L *et al* 2012 Field-effect tunneling transistor based on vertical graphene heterostructures *Science* **335** 947–50
[17] Novoselov K S, Mishchenko A, Carvalho A and Castro Neto A H 2016 2D materials and van der Waals heterostructures *Science* **353** aac9439
[18] Yu W J, Liu Y, Zhou H, Yin A, Li Z, Huang Y and Duan X 2013 Highly efficient gate-tunable photocurrent generation in vertical heterostructures of layered materials *Nat. Nanotechnol.* **8** 952–8
[19] Deng Y, Luo Z, Conrad N J, Liu H, Gong Y, Najmaei S, Ajayan P M, Lou J, Xu X and Ye P D 2014 Black phosphorus-monolayer MoS_2 van der Waals heterojunction p-n diode *ACS Nano* **8** 8292–9
[20] Yuan J, Najmaei S, Zhang Z, Zhang J, Lei S, Ajayan P M, Yakobson B I and Lou J 2015 Photoluminescence quenching and charge transfer in artificial heterostacks of monolayer transition metal dichalcogenides and few-layer black phosphorus *ACS Nano* **9** 555–63

[21] Hu W, Wang T and Yang J 2015 Tunable Schottky contacts in hybrid graphene-phosphorene nanocomposites *J. Mater. Chem.* C **3** 4756–61
[22] Kumar R, Das D and Singh A K 2018 C_2N/WS_2 van der Waals type-II heterostructure as a promising water splitting photocatalyst *J. Catalysis* **359** 143–50
[23] Huang L, Huo N, Li Y, Chen H, Yang J, Wei Z, Li J and Li S-S 2015 Electric-field tunable band offsets in black phosphorus and MoS_2 van der Waals pn heterostructure *J. Phys. Chem. Lett.* **6** 2483–8
[24] Chen X, Tan C, Yang Q, Meng R, Liang Q, Jiang J, Sun X, Yang D and Ren T 2016 Effect of multilayer structure, stacking order and external electric field on the electrical properties of few-layer boron–phosphide *Phys. Chem. Chem. Phys.* **18** 16229–36
[25] Talapin D V, Mekis I, Götzinger S, Kornowski A, Benson O and Weller H 2004 CdSe/CdS/ZnS and CdSe/ZnSe/ZnS core–shell–shell nanocrystals *J. Phys. Chem.* B **108** 18826–31
[26] Lukashev P V, Paudel T R, Lopez-Encarnacion J M, Adenwalla S, Tsymbal E Y and Velev J P 2012 Ferroelectric control of magnetocrystalline anisotropy at cobalt/poly(vinylidene fluoride) interfaces *ACS Nano* **6** 9745–50
[27] Rinaldi C *et al* 2018 Ferroelectric control of the spin texture in GeTe *Nano Lett.* **18** 2751–8
[28] Meng Y-H, Bai W, Gao H, Gong S-J, Duan C-G and Chu J-H 2017 Ferroelectric control of the giant Rashba spin–orbit coupling in GeTe (1 1 1)/InP (1 1 1) superlattice *Nanoscale* **9** 17957–62
[29] Zhou Y, Wu D, Zhu Y, Cho Y, He Q, Yang X, Herrera K, Chu Z, Han Y and Downer M C 2017 Out-of-plane piezoelectricity and ferroelectricity in layered α-In_2Se_3 nanoflakes *Nano Lett.* **17** 5508–13
[30] Cui C, Hu W-J, Yan X, Addiego C, Gao W, Wang Y, Wang Z, Li L, Cheng Y and Li P 2018 Intercorrelated in-plane and out-of-plane ferroelectricity in ultrathin two-dimensional layered semiconductor In_2Se_3 *Nano Lett.* **18** 1253–8
[31] Zheng C, Yu L, Zhu L, Collins J L, Kim D, Lou Y, Xu C, Li M, Wei Z and Zhang Y 2018 Room temperature in-plane ferroelectricity in van der Waals In_2Se_3 *Sci. Adv.* **4** eaar7720
[32] Ding W, Zhu J, Wang Z, Gao Y, Xiao D, Gu Y, Zhang Z and Zhu W 2017 Prediction of intrinsic two-dimensional ferroelectrics in In_2Se_3 and other III_2–VI_3 van der Waals materials *Nat. Commun.* **8** 14956
[33] Debbichi L, Eriksson O and Lebegue S B 2015 Two-dimensional indium selenides compounds: an *ab initio* study *J. Phys. Chem. Lett.* **6** 3098–103
[34] Zhang Y B, Tang T T, Girit C, Hao Z, Martin M C, Zettl A, Crommie M F, Shen Y R and Wang F 2009 Direct observation of a widely tunable bandgap in bilayer graphene *Nature* **459** 820–3
[35] Lui C H, Li Z Q, Mak K F, Cappelluti E and Heinz T F 2011 Observation of an electrically tunable band gap in trilayer graphene *Nat. Phys.* **7** 944–7
[36] Blochl P E 1994 Projector augmented-wave method *Phys. Rev.* B **50** 17953
[37] Kresse G and Furthmüller J R 1996 Efficient iterative schemes for *ab initio* total-energy calculations using a plane-wave basis set *Phys. Rev.* B **54** 11169
[38] Perdew J P, Burke K and Ernzerhof M 1996 Generalized gradient approximation made simple *Phys. Rev. Lett.* **77** 3865
[39] Grimme S 2006 Semiempirical GGA-type density functional constructed with a long-range dispersion correction *J. Comput. Chem.* **27** 1787–99
[40] Kerber T, Sierka M and Sauer J 2008 Application of semiempirical long-range dispersion corrections to periodic systems in density functional theory *J. Comput. Chem.* **29** 2088–97
[41] Monkhorst H J and Pack J D 1976 Special points for Brillouin-zone integrations *Phys. Rev.* B **13** 5188
[42] Demirci S, Avazlí N, Durgun E and Cahangirov S 2017 Structural and electronic properties of monolayer group III monochalcogenides *Phys. Rev.* B **95** 115409
[43] Li X, Li Z and Yang J 2014 Proposed photosynthesis method for producing hydrogen from dissociated water molecules using incident near-infrared light *Phys. Rev. Lett.* **112** 018301
[44] Ahn C H, Rabe K M and Triscone J M 2004 Ferroelectricity at the nanoscale: local polarization in oxide thin films and heterostructures *Science* **303** 488–91
[45] Dawber M, Rabe K M and Scott J F 2005 Physics of thin-film ferroelectric oxides *Rev. Mod. Phys.* **77** 1083
[46] Henkelman G, Arnaldsson A and Jonsson H 2006 A fast and robust algorithm for Bader decomposition of charge density *Comput. Mater. Sci.* **36** 354–60
[47] Lo S S, Mirkovic T, Chuang C H, Burda C and Scholes G D 2011 Emergent properties resulting from type-II band alignment in semiconductor nanoheterostructures *Adv. Mater.* **23** 180–97
[48] Palummo M, Bernardi M and Grossman J C 2015 Exciton radiative lifetimes in two-dimensional transition metal dichalcogenides *Nano Lett.* **15** 2794–800